Pan-genome and antibiotic resistance insights into Xanthomonas citri pv. punicae pathotypes

Rathna, V.; Kukreti, Aditya; Prasannakumar, M. K.; Manjunatha, C.; Karan, R.; Patil, Swathi S.; Venkateshbabu, Gopal; Devanna, Pramesh; Harish, J.; Banakar, Sahana N.; Sarangi, Aditya Narayan; Vaidya, Keerthi; Rymbai, Shibormi; Mahesh, H. B.; Soolanayakanahally, Raju Y.; Kagale, Sateesh

Publisher's version / Version de l'éditeur:

https://doi.org/10.1186/s12866-025-04625-w

BMC Microbiology, 26, 1, 2026-01-16

BMC Microbiology

RESEARCH

Open Access

Pan-genome and antibiotic resistance insights into *Xanthomonas citri* pv. *punicae* pathotypes

Rathna V.[1], Aditya Kukreti[2], M. K. Prasannakumar[1*], Manjunatha C.[2], Karan R.[1], Swathi S. Patil[1], Gopal Venkateshbabu[1], Pramesh Devanna[3], Harish J.[1], Sahana N. Banakar[1], Aditya Narayan Sarangi[4], Keerthi Vaidya[4], Shibormi Rymbai[4], H. B. Mahesh[1], Raju Y. Soolanayakanahally[5] and Sateesh Kagale[6]

Abstract

Background Bacterial blight, caused by *Xanthomonas citri* pv. *punicae* (Xcp) is a significant threat to pomegranate cultivation in India. Although antibiotics such as streptomycin, streptocycline, and tetracycline are commonly used for its management, their effectiveness is declining due to the emergence of resistant Xcp strains carrying acquired resistance genes. Considering this growing concern, the present study aimed to investigate nine Xcp isolates obtained from pomegranate-growing regions of India by assessing their pathogenicity, followed by in vitro evaluation of their antibiotic sensitivity, and subsequently analyzing their antibiotic resistance gene (ARG) profiles and genome diversity through whole-genome sequencing.

Results Morphological and 16 S rRNA sequencing analyses confirmed that all Xcp strains shared 98.5–100% nucleotide identity with *X. citri*. Pathogenicity assays identified Xcp1 as the most virulent strain. Antibiotic sensitivity tests showed that Xcp1 was most sensitive to streptomycin, while Xcp3 and Xcp9 were more susceptible to tetracycline. Whole-genome sequencing revealed genome sizes of 4.72–4.93 Mb, a GC content of ~65%, and ≥ 99% ANI with *X. citri* LMG 859. Across the nine Xcp strains, 6,623 to 6,925 genes were annotated with Gene Ontology and grouped into 44 subclasses within three main functional categories. The ARG profiling of nine Xcp strains revealed a conserved set of three chromosomal resistance genes, including *vanY* and *adeF*, along with diverse putative ARGs and variable plasmid-associated elements. Prediction of Type III secretion system (T3SS) proteins in nine Xcp strains revealed well-characterized proteins such as XopI, XopA, XopN, XopX, XopL, XopR, XopAV, XopK, XopAE, XopQ, XopP, XopAP, as well as avirulence-associated proteins like AvrBs2 and other LRR-type effectors, highlighting their likely critical role in Xcp pathogenicity. BRIG analysis using Xcp1 as the reference genome revealed near-complete (~100%) similarity across most genomic regions of the eight isolates. However, a 500 kb region between 4.5 and 5.0 Mbp showed reduced similarity (~70%) in five isolates. Further analysis using Mauve alignments indicated that only Xcp3 and Xcp9 contained additional homologous blocks in this region, suggesting strain-specific structural variations. In contrast, the similarity drop in Xcp2, Xcp4, and Xcp5 corresponded to contig boundaries without changes in gene order, indicating these were likely assembly artifacts rather than true genomic rearrangements.

*Correspondence:
M. K. Prasannakumar
babu_prasanna@rediffmail.com

Full list of author information is available at the end of the article

Conclusions This study highlights genomic and phenotypic variation among Xcp strains, revealing strain-specific virulence, resistance genes, and genomic rearrangements. The findings enhance our understanding of Xcp adaptation and resistance, offering a foundation for improved disease management strategies in India.

Keywords Whole genome sequencing, Pomegranate, Streptomycin, Streptocycline, Tetracycline

Background

Pomegranate (*Punica granatum* L.) is a highly valued horticultural crop known for its nutritional and medicinal properties [1]. India is the world's leading producer of pomegranate, cultivating an extensive 283 thousand hectares and achieving an annual yield of 3.186 million tons [2]. Over the past decade, bacterial blight, commonly known as oily spot disease, caused by *Xanthomonas citri* pv. *punicae* (Xcp), and previously referred to as *X. axonopodis* pv. *punicae* (Xap) has emerged as a major threat to pomegranate farming in India [3]. This disease affects all aerial parts of the plant, including the stems, leaves, flowers, fruits, and buds, with fruits being the most severely impacted [4]. Under favorable conditions, it can cause yield losses ranging from 60% to 80% [5].

Bhagwa, a popular pomegranate variety in India, dominates over 86% of the country's pomegranate cultivation due to its high demand in both domestic and international markets. Its popularity is evident in its remarkable growth in cultivation area (108.93%), production (268.53%), and export value (455.68%) since 2003–04. However, Bhagwa is highly susceptible to Xcp. With no resistant cultivars available, farmers often resort to excessive chemical application to control the disease, further exacerbating the problem [2].

The bacterial blight of pomegranate has been managed in the field using streptocycline, a combination of 90% streptomycin sulfate and 10% tetracycline hydrochloride, applied at 0.5 g/L, often along with other bactericides like bronopol. However, its effectiveness has declined in recent years due to excessive use [6]. One of the primary reasons for this reduced efficacy is the emergence of antibiotic resistance in the bacterial population, driven by selection pressure from repeated exposure [2, 6]. Limited information is available on the sensitivity of Xcp to streptomycin and there are no documented cases of Xcp exhibiting resistance to tetracycline or streptomycin sulfate [7–9].

Comprehensive genomic studies are essential for tackling the challenges of antibiotic resistance by uncovering genetic markers linked to both resistance and pathogenicity. By integrating whole genome sequencing data from pathogenic strains, we can gain deeper insights into the mechanisms driving resistance, enabling the development of more targeted and sustainable disease management strategies. In recent years, this approach has been widely used to study various bacterial plant pathogens, helping to uncover phylogenetic relationships, genetic factors responsible for pathogenicity, and potential diagnostic markers [10]. The vast amount of data generated through whole genome sequencing has provided valuable opportunities to examine infection strategies, track pathogen movement, and link phenotypic traits to targeted disease management approaches [11].

A major challenge in understanding the development of pathogenicity and antibiotic resistance in Xcp is the lack of comprehensive genomic resources. At the time of initiating this study, only 14 assembled genomes of Xcp were publicly available in the NCBI GenBank/RefSeq databases, of which two were based on long-read sequencing and the remaining 12 on short-read sequencing. As part of this study, we have submitted an additional nine genome assemblies, bringing the current total to 23. Therefore, a detailed whole genome study of Xcp is essential to enhance current datasets with novel strains and high-quality sequencing data. This could significantly improve the accuracy of genome assemblies, facilitate gene identification, and expand our understanding of gene families associated with pathogenicity and antibiotic resistance [11].

Like other *Xanthomonas* species and most Gram-negative bacteria, Xcp utilizes type 3 secretion systems (T3SS) to transfer crucial pathogenicity effectors into host cells [12]. Genomic studies on Xcp can provide valuable insights into its virulence mechanisms, shedding light on plasmids, secretion systems, host interaction effectors, carbohydrate-active enzymes, cell wall-degrading enzymes, and antibiotic and antimicrobial resistance pathways. Understanding these genetic factors can pave the way for more effective disease control strategies and the development of resistant cultivars.

Despite significant progress in genomic research, no study has yet investigated antibiotic resistance in *Xanthomonas citri* pv. *punicae* (Xcp) through comparative genomics. To bridge this gap, we conducted whole genome sequencing of nine Xcp strains isolated from pomegranate-growing regions across Karnataka, New Delhi, Maharashtra, and Andhra Pradesh, India. Using a combination of Illumina and Oxford Nanopore sequencing technologies (ONT), we generated high-quality, closed genome assemblies, enhancing the accuracy of genetic analyses. This study further provides critical insights into antibiotic resistance genes (ARGs), antimicrobial resistance mechanisms, secretomes, type 3 secretion systems (T3SS), transposons, and pathogenicity islands. By comparing whole genomes of different

Xcp isolates, our findings contribute to a deeper understanding of the pathogen's genetic diversity, virulence, and potential strategies for more effective disease management.

Materials and methods

Collection and morphological characterization of Xcp

Leaf samples exhibiting characteristic bacterial blight symptoms in pomegranate (initial small 2–5 mm, irregular, water-soaked lesions, which progressed to necrotic spots with light to dark brown centers surrounded by prominent water-soaked margins) were collected from cultivar Bhagwa from different geographical regions of India (Table 1). A total of nine Xcp strains were used in the study. For isolation, the collected leaf samples were surface-sterilized with 2% sodium hypochlorite, then thoroughly rinsed with sterile deionized water and dried by blotting. The plant tissue was then macerated and streaked onto nutrient agar (NA) plates, which were incubated at 28 ± 1 °C for 48 h. After the incubation period, colonies that appeared were selected based on their colour, texture, morphology, and distinct pigmentation features.

Pathogenicity test and disease severity of Xcp isolates

The six-month-old pomegranate seedlings (cv. Bhagwa) susceptible to bacterial blight were used for pathogenicity studies. The healthy seedlings, grown in polythene bags, were transplanted into sterilized soil and preconditioned by water spraying and incubation for 24 h in a moist glasshouse (28 ± 2 °C, 70% RH). A single colony of Xcp 1–9 strains was cultured in nutrient broth (NB) with 1% glucose at 28 °C and 120 rpm for 48 h to obtain an inoculum (0.3 OD600, ~10^5 CFU/mL). A constant volume of 50 µL was used for each infiltration point across all treatments using a micropipette to maintain uniformity. A consistent infiltration area was selected and marked on all host plants. Inoculations were performed using a syringe without a needle, ensuring minimal variation in pressure and penetration depth. Control plants were treated with sterilized distilled water. The inoculated plants were regularly sprayed with water, and symptoms (water-soaked lesions) were observed 7–10 days post-inoculation (DPI). For each isolate, the experiment included three replications to ensure the reproducibility and statistical robustness of the disease severity comparisons. To confirm pathogenicity, the pathogen was re-isolated from the infected plants and compared with the original culture.

Quantitative PCR based virulence assessment

Genomic DNA was extracted from the infected leaf tissues at 8 days post-inoculation (DPI) using a standard Cetyltrimethylammonium bromide (CTAB) method. Quantitative PCR (qPCR) was performed using primers specific to the *xopQ*, which encodes a type III effector (Forward: 5′-GCGAGGAACTTGGAATGCTC-3′; Reverse: 5′-AGGTCGAAGGCTTTTTGCG-3′) [13]. The qPCR amplification was carried out in a thermal cycler under the following conditions: initial denaturation at 94 °C for 4 min, 35 cycles of denaturation at 94 °C for 15 s, annealing at 58 °C for 30 s, and extension at 72 °C for 45 s; followed by a final extension at 72 °C for 10 min. Cycle threshold (Ct) values obtained were compared against a standard curve generated using known concentrations of target DNA, and the bacterial load was quantified as DNA copy number per sample.

In vitro bioassay for antibiotic sensitivity of Xcp by the disc diffusion method

The antibiotics streptomycin sulfate (Ambistryn), streptocycline (K-cyclin) and tetracycline were used at different concentrations to assess their effects on Xcp isolates via disc diffusion method. For each of the antibiotics, treatments included a range of antibiotic concentrations as follows: T1 (50 µg/mL), T2 (100 µg/mL), T3 (200 µg/mL), T4 (400 µg/mL), T5 (600 µg/mL), T6 (800 µg/mL), T7 (1000 µg/mL), T8 (1500 µg/mL), T9 (2000 µg/mL), T10 (3000 µg/mL), T11 (4000 µg/mL), and T12 (5000 µg/mL). A control using sterile distilled water was also included to serve as a baseline for comparison. For the disc diffusion method, nine Xcp strains were inoculated in the nutrient broth with 1% glucose to prepare inoculum suspensions, followed by incubation in a shaker at 27 ± 2 °C for three days at 120 rpm. Sterilized, oven-dried 5 mm filter paper discs were soaked in antibiotic solutions for 30 min, then placed onto Petri plates containing solidified nutrient medium seeded with the bacterial culture. Each Petri plate contained three discs per antibiotic concentration, arranged in a triangular pattern, which were technical replicates for each treatment within a plate. The experiment was conducted using three biological replicates per Xcp isolate, and the entire assay was repeated twice independently. After refrigeration at 5 °C for 2 h, plates were incubated at 27 ± 2 °C. The zones of inhibition were measured after 48–72 h. A complete randomized design (CRD) was employed for two-way factor analysis using R software [14]. The analysis and data manipulation were performed using the dplyr [15] and tidyr [16] packages for data wrangling. The bar plot with standard deviation error bars was created using the ggplot2 [17] package for visualization.

DNA extraction and molecular confirmation via 16 S rRNA sequencing

The genomic DNA was extracted from 48 h old culture of Xcp strains grown in nutrient broth using the DNeasy Blood and Tissue Kit (Qiagen, Hilden, Germany),

Table 1 General genome features of *Xanthomonas citri* pv. *punicae* strains Xcp1–Xcp9. ANI values (compared with the closest organism *X. citri* strain LMG 859) range from 99.86 to 99.93. All genomes correspond to bioproject ID: PRJNA865108

Isolates	Xcp1	Xcp2	Xcp3	Xcp4	Xcp5	Xcp6	Xcp7	Xcp8	Xcp9
Location	Davanagere, Karnataka	Davanagere, Karnataka	New Delhi	New Delhi	Solapur, Maharashtra	New Delhi	New Delhi	New Delhi	Anantapur, Andhra Pradesh
Total Contigs	5	4	5	5	5	5	5	4	5
Large chromosomal region	1	1	1	1	1	1	1	1	1
Plasmid regions	2	0	1	1	1	1	1	0	1
Small chromosomal fragments	2	3	3	3	3	3	3	3	3
Largest contig	4,719,958	4,591,006	4,584,439	4,588,948	4,611,596	4,611,133	4,611,226	4,624,623	4,582,864
Total length (bp)	4,934,678	4,721,840	4,727,928	4,732,435	4,755,081	4,758,651	4,760,982	4,760,312	4,726,351
N50	4,719,958	4,591,006	4,584,439	4,588,948	4,611,596	4,611,133	4,611,226	4,624,623	4,582,864
N75	4,719,958	4,591,006	4,584,439	4,588,948	4,611,596	4,611,133	4,611,226	4,624,623	4,582,864
GC (%) of chromosome	64.87	65.11	65.11	65.11	65.1	65.09	65.09	65.08	65.11
Predicted rRNA genes	3 + 0 part	0 + 0 part	0 + 0 part	0 + 0 part	0 + 0 part	0 + 0 part	0 + 0 part	0 + 0 part	0 + 0part
16 S rRNA accession ID	PV093904	PV093905	PV093906	PV093907	PV093908	PV093909	PV093910	PV093911	PV093912
GenBank accession number	JAODJP000000000	JAODJO000000000	JAODJN000000000	JAODJM000000000	JAODJL000000000	JAODJK000000000	JAOD-JJ000000000	JAOD-JI000000000	JAOD-JH000000000
Biosample accession	SAMN30096794	SAMN30096795	SAMN30096796	SAMN30096797	SAMN30096798	SAMN30096799	SAMN30096800	SAMN30096801	SAMN30096802

following the manufacturer's protocol. The amplified DNA products were visualized in 1% agarose gel and observed under the gel documentation system (DNR, MiniLumi, Israel). The genomic DNA was preserved following assessment of purity and concentration using a NanoDrop™ spectrophotometer (Thermo Fisher Scientific, USA), at 20 °C for further use.

The identification of the six bacterial isolates was carried out by amplifying the 16 S rRNA region using the primers 27 F (AGAGTTTGATCMTGGCTCAG) and 1492R (GGTTACCTTGTTACGACTT). PCR was performed with the following thermal cycling conditions: initial denaturation at 94 °C for 5 min, followed by 35 cycles of denaturation at 94 °C for 30 s, annealing at 57 °C for 30 s, and extension at 72 °C for 30 s, with a final extension at 72 °C for 10 min. The amplified PCR products were purified *via* ExoSAP-IT™ Express PCR Product Cleanup (Thermo Fisher Scientific, USA), followed by Sanger sequencing. The obtained forward and reverse reads were then aligned and assembled using the ClustalW [18] tool in BioEdit v. 7.2.5 [19] before proceeding with BLAST analysis for sequence identification. Phylogenetic relationships were inferred through the neighbor-joining method with 1,000 bootstrap replicates in MEGA 11 [20].

Illumina and ONT library preparation

Genome sequencing was carried out for all nine Xcp strains using the Illumina NextSeq 500 platform (Illumina Inc., San Diego, CA). To prepare the DNA Illumina library, 1 µg of genomic DNA was mechanically sheared using microTUBE AFA Fiber Snap-Cap tubes (Thermo Fisher Scientific, USA) on the M220 Focused Ultrasonicator (Covaris, Woburn, MA, USA). DNA fragments approximately 350 bp in length were then selected with the AMpure purification kit (Beckman Coulter Life Sciences, USA), and sequencing libraries were prepared using the NEBNext® Ultra™ II DNA Library Prep kit (New England Biolabs, USA) according to the manufacturer's guidelines. The size-selected DNA underwent PCR amplification with index primers, after which indexing adapters were ligated to the ends of the fragments to enable hybridization on a flow cell. The enriched libraries were subsequently analyzed on the Agilent 4200 TapeStation system using high-sensitivity D1000 ScreenTape as instructed by the manufacturer. After measuring the Qubit concentration and determining the mean peak sizes, the paired-end Illumina libraries were loaded onto the NextSeq500 system for cluster generation and sequencing. The ONT sequencing was carried out only for the Xcp1 strain. The library was prepared using the ONT nonbarcoding kit (SQK-RAD004) and run twice in MinION flow cells (v. R9.4.1) for approximately 22 h each time to obtain sufficient coverage [21].

Genome assembly

The raw data obtained from Illumina sequencing of the nine Xcp strains genomes Xcp1-Xcp9 underwent processing using FastQC v0.11.9, and low-quality bases and adapter contaminations were filtered using Trimmomatic v0.39 (parameters: -f 3, -q 15 -c) and Fastp v.0.20.1 (parameters: -f 10 -q 30 -c) [22–24]. The initial quality assessment of ONT data for Xcp1 was conducted using NanoQC v.0.9.4, and the data were subsequently filtered with NanoFilt v.2.8.0 (parameters: -q 8 -l 1000) [25].

A hybrid assembly for Xcp1 based on the filtered Illumina paired-end reads and ONT reads was done with Unicycler v.0.4.4 (parameters: --min_fasta_length 1000–mode normal) [26]. Reference-based scaffolding of the *de-novo* assembly of Xcp1 was done using Reference-guided Genome Ordering and Orientation (RaGOO) [27] based on *Xanthomonas citri* pv. punicae reference genome assembly (ASM622842v1).

De-novo assembly of Illumina sequences of Xcp2-Xcp9 was performed based on the processed reads using SKESA v.2.4.0 (with varying --min-contig parameters 200, 500, and 1000, where assembly generated with parameters–min-contig 1000 showed better assembly quality as evidenced by higher N_{50} values and reduced fragmentation) [28]. Draft genome binning was carried out using MetaBat2 and the recovered genome bins were subjected to CheckM v.1.1 to estimate the contamination level and completeness of the recovered genome bins [29, 30]. The contamination free complete genome bins were scaffolded based on the Xcp1 scaffolded assembly as reference using RaGOO.

Genome annotation

The genome assembly quality assessment was done using QUAST v.5.0.2 [31]. Annotation of the scaffolded assembled genomes (Xcp1-Xcp9) was done using Prokka v.1.14.6 [32]. These Prokka outputs were used for all downstream analyses presented in this study. While the NCBI GenBank record contains annotations generated by PGAP (Prokaryotic Genome Annotation Project), the Prokka annotation dataset has been deposited as Supplementary Files to ensure reproducibility and transparency. Average Nucleotide Identity (ANI) was calculated using FastANI (parameters: fastANI -q XAP1.fasta -r GCA_000285775.1.fna -o fastani_output.txt -t 8) to infer genomic relatedness for taxonomic placement, and completeness and rate of contamination were assessed based on CheckM implemented in DFAST online server [33]. Ab-initio prediction of non-classical secretory proteins (not signal peptide triggered protein secretion) was done using the Effective T3 v.1.0.1 (parameters: java -jar EffectiveT3_v1.0.1.jar -m TTSS_PLANT-1.0.1.jar -t cut-off = 0.995 -q input.faa) [34]. Platon v.1.5.0 (platon --db /path/to/platon_db -f assembly.fasta -o platon_output/)

was used to identify and characterize bacterial plasmid contigs [35]. The Gene Ontology (GO) annotation and identification of GO terms were done by subjecting the protein sequences to PANNZER2 (http://ekhidna2.biocenter.helsinki.fi/sanspanz/) [36]. For GO enrichment, this GO output was subjected to WEGO (https://wego.genomics.cn/) [37]. The pathway analysis was carried out using the KEGG automatic annotation server (https://www.genome.jp/tools/kaas/) [38]. The detection-based profiling of virulence and antibiotic resistance traits encoded within genome sequences was done using VRprofile (https://tool2-mml.sjtu.edu.cn/VRprofile), followed by a submission to CGview (java: -jar CGView.jar -i genome.gbk -o genome_circular_map.png) to generate the circular genome plot [39]. The similarity values between two or more genome sequences were done using OrthoANI (Orthologous Average Nucleotide Identity) (python: orthoani.py -q genome1.fasta -r genome2.fasta -o output_dir) [40].

The assembled fasta files were submitted to ISsaga (https://www-is.biotoul.fr/) for annotation of the insertion sequence [41]. Identification of the transposase insertion sequence location was done by using ISmapper v.2.0.1 (ismapper.py -i reads.fastq.gz -r reference.fasta -s IS_sequences.fasta -o output_dir) [42]. Variant calling was done by using Snippy v.4.6 (snippy --cpus 8 --outdir snippy_out --ref reference.fasta --R1 reads_1.fastq.gz --R2 reads_2.fastq.gz) [43]. Pathogenicity Island viewer was done using Island Viewer 4 (https://www.pathogenomics.sfu.ca/islandviewer/) with a GenBank file [44].

Phylogenetic and evolutionary analysis of Xcp isolates

The pangenome analysis of the 19 Xcp strains (Xcp-1 to Xcp-9, Xcp-118, Xcp-119, Xcp-Bagalkot, Xcp-BD0022, Xcp-BD0023, Xcp-BD0025, Xcp-LMG7439, Xcp-LMG7504, Xcp-LMG859, and Xcp-NCPPB3563) was done using the Bacterial Pan Genome Analysis Tool (BPGA) v.1.3 (perl BPGA.pl -f protein_fasta_list.txt -a USEARCH -t 0.5 -o output_dir) [45]. BPGA performs evolutionary analysis using concatenated core gene alignments and a binary pan-matrix based on gene presence/absence across orthologous clusters. It excludes paralogs and selects 20 random core gene clusters for phylogenetic tree construction using MUSCLE alignments. The phylogeny was inferred using the Maximum Likelihood method and Jones-Taylor-Thornton (1992) model [46]. Evolutionary analyses were conducted in MEGA 11 [20]. The accessory gene-based phylogenetic tree was generated using PanExplorer [47], based on the Neighbor-Joining (NJ) method.

Prediction of T3 effectors

Putative effector proteins were identified using Effectidor II (https://effectidor.tau.ac.il/) [48] with default parameters, based on genome annotations generated through Bakta (https://bakta.computational.bio/). The Bakta annotation output, including the predicted protein FASTA and GFF3 files, was provided as input to Effectidor II, which integrates multiple sequence-based features and classifiers to detect candidate effectors. The pipeline, executed in default mode, incorporated signal peptide prediction (SignalP), transmembrane domain filtering (TMHMM), domain searches against Pfam-A, CDD, and effector-specific HMM profiles, as well as subcellular localization prediction and machine learning–based scoring of effector likelihood. Default parameters were applied throughout the run. The resulting effector candidate list, including predicted homologs, scores, and feature annotations, was used for downstream comparative and functional analyses.

Prediction of antibiotic resistance genes

The draft genome assemblies of individual Xcp strains were separated into chromosomal and plasmid-derived contigs using PlasFlow [49]. Subsequently, ARGs were identified on each component using the Comprehensive Antibiotic Resistance Database - Resistance Gene Identifier (CARD-RGI) tool [50], applying both strict and loose detection criteria. Circular maps representing the AMR detected by the CARD Resistance gene identifier (RGI) were generated using the Proksee server (https://proksee.ca/) [51].

Whole genome comparison

Illumina sequences of Xcp1-9 strains were compared using BLAST Ring Image Generator (BRIG) v.0.95 (java -jar BRIG.jar), which used CGView for image rendering and BLAST for genome comparisons [52, 53]. The Mauve genome alignment program was employed to address the issue of genome rearrangements and contig ordering of the draft genomes by pairwise comparison [54].

Results

Pathogenicity and disease severity of Xcp isolates

A total of nine Xcp strains were isolated from leaf samples showing typical bacterial blight symptoms in pomegranate collected from cultivar Bhagwa across various geographical regions in India, including Davanagere (Karnataka), New Delhi, Solapur (Maharashtra), and Ananthpur (Andhra Pradesh). The pure cultures of the nine strains exhibited typical Xcp growth characteristics, forming yellow, mucoid, and circular colonies. When inoculated on pomegranate leaves, the Xcp isolates induced characteristic symptoms, beginning with small water-soaked spots that gradually turned brown to dark brown. These spots were surrounded by a diffused water-soaked margin or yellow halo, forming circular to irregular lesions (Fig. 1a). As the disease progressed, the spots

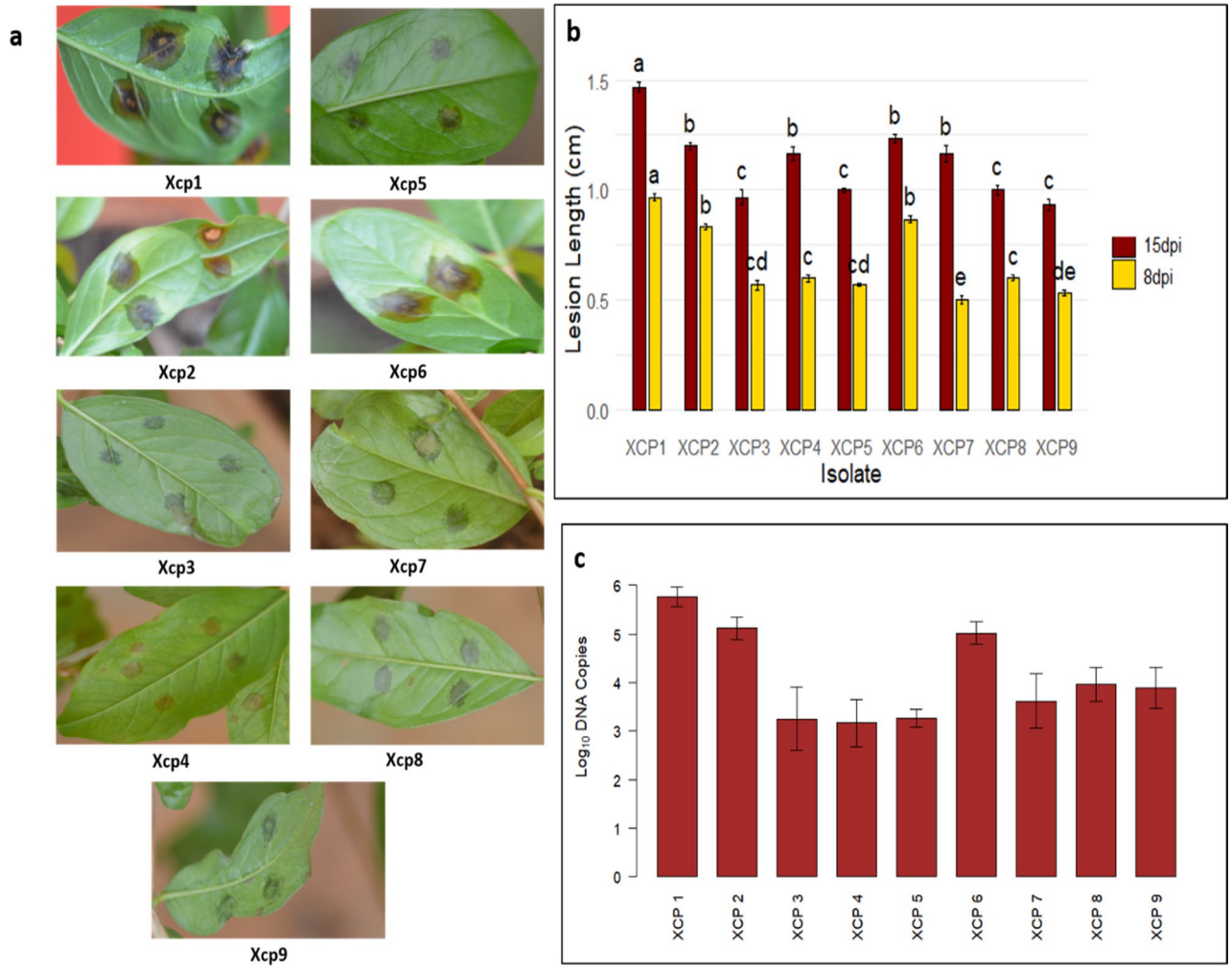

Fig. 1 Virulence assessment of Xcp strains in pomegranate. **a** Representative symptoms on pomegranate leaves at 15 DAI with different Xcp strains, showing variation in lesion size; (**b**) Lesion lengths (cm) induced by XCP strains at 8 dpi and 15 dpi with error bars showing ± SE. Statistical differences among strains were assessed using one-way ANOVA ($p < 0.001$) followed by Duncan's Multiple Range Test (DMRT, $\alpha = 0.05$), where different lowercase letters above bars indicate statistically significant differences ($p < 0.05$) among lesion lengths induced by each strain. Identical letters denote no significant difference; (**c**) Quantification of in planta bacterial load at 8 DAI using qPCR targeting the *xopQ* effector gene. DNA copy numbers are presented as $\log_{10}$-transformed values

expanded, leading to necrosis. Re-isolation from the inoculated leaves displaying typical bacterial blight symptoms confirmed the pathogenicity. The cultures obtained through serial dilution on the NA medium resembled the original cultures, confirming the pathogen's identity (Fig. 1a).

The disease severity and virulence of the isolates were assessed by measuring the lesion length in the necrotic areas. Among all isolates, Xcp1 exhibited the highest virulence, showing lesion lengths of 0.9 cm at 8 dpi and 1.4 cm at 15 dpi. In contrast, the Xcp9 isolate exhibited the lowest virulence, with smaller lesions compared to Xcp1 (Fig. 1b, Table S2).

Quantitative PCR based virulence assessment

To complement lesion measurements, *in planta* bacterial populations were quantified using qPCR targeting the *xopQ* gene. DNA was extracted from infected leaves at 8 days after inoculation (DAI), and $\log_{10}$-transformed DNA copy numbers were estimated based on a standard curve. Results showed a strong correlation between lesion severity and bacterial DNA copy number (Fig. 1c, Fig. S1d). Xcp1 and Xcp2 exhibited the highest bacterial loads, with log DNA copy numbers exceeding 5.0, while Xcp4 and Xcp5 showed significantly lower bacterial abundance (~ 3.0–3.5 log copies), consistent with their lower virulence phenotype.

In vitro antibiotic sensitivity testing of Xcp using the disc diffusion method

The sensitivity of Xcp strains to streptomycin sulfate was evaluated across concentrations ranging from 50 to 5000 ppm, with the inhibition zone generally increasing as the concentration increased. At 50 ppm, Xcp1 showed the largest inhibition zone of 0.97 cm, while Xcp4, Xcp5, and Xcp9 had the smallest inhibition zones of 0.60 cm. At higher concentrations, inhibition zones continued to expand, reaching the highest recorded at 5000 ppm, where Xcp1 showed a maximum inhibition zone of 3.63 cm, and Xcp8 had the smallest zone at 2.90 cm. Overall, Xcp1 demonstrated the greatest susceptibility to streptomycin, while Xcp7 and Xcp9 exhibited lower susceptibility. Although there was little variation in inhibition at lower concentrations, significant differences were observed at higher concentrations, suggesting that Xcp isolates respond more strongly to increasing streptomycin sulfate concentrations (Fig. S1a, 2a).

Similarly, streptocycline sensitivity of Xcp isolates was evaluated by measuring the inhibition zone across concentrations ranging from 50 to 5000 ppm. At 50 ppm, Xcp1, Xcp2, and Xcp6 showed slight inhibition, while most isolates exhibited no inhibition. As the concentration increased, Xcp6 displayed the highest sensitivity, with inhibition zones reaching 2.77 cm at 5000 ppm, while Xcp8 and Xcp9 showed minimal response, indicating lower susceptibility across all concentrations (Fig. S1b, 2b).

In the tetracycline sensitivity assays, Xcp3 showed the highest inhibition (1.47 cm), followed by Xcp9 (1.33 cm), while Xcp1 exhibited no inhibition at 50 ppm. As concentrations increased, Xcp3 and Xcp9 consistently demonstrated the highest sensitivity, with inhibition zones reaching up to 3.67 cm at 5000 ppm, while Xcp4 showed the least susceptibility with lower inhibition zones (Fig. S1c, 2c).

Molecular confirmation via 16S rRNA sequencing

A phylogenetic tree constructed based on 16S rRNA gene sequences revealed that the isolates are clustered into two clades and are closely related and clustered within the Xcp, indicating their genetic similarity to it, and the sequences were submitted to the GenBank NCBI database, and accession numbers were obtained (Table 1, Fig. S2).

Genome assembly and annotation

The genomes of nine Xcp strains were sequenced and assembled using Illumina, while the genome of the most virulent strain, Xcp1, was assembled through a hybrid approach combining Illumina short reads with ONT long reads. Assembly quality and completeness, assessed using CheckM, indicated 98.07–100% completeness with negligible contamination. The final draft genome assemblies of Xcp1-9 consisted of a single circular chromosome ranging from 4.72 Mb to 4.93 Mb, with an average GC content of 64.87–65.11%. Extrachromosomal contigs ranged from 7.79 to 82.86 kb with 0–2 plasmid hits observed across all the isolates (Table 1). The N50 values ranged from 4.58 to 4.71 Mb, with 0–3 predicted rRNA genes. The identity of the strains as Xcp was verified using the DFAST tool. The analysis of average nucleotide identity (ANI) confirmed high similarity among the nine Xcp strains. The Xcp strains shared the highest ANI (≥ 99%) with *X. citri* strain LMG 859 (accession no. GCA_000285775.1). Detailed assembly statistics and annotation features of these genomes are listed in Table 1. The annotated genomes of Xcp strains 1–9 have been deposited in the NCBI database.

The GO analysis yielded a total of 6925 (Xcp1), 6721 (Xcp2), 6623 (Xcp3), 6629 (Xcp4), 6744 (Xcp5), 6744 (Xcp6), 6735 (Xcp7), 6738 (Xcp8) and 6627 (Xcp9) genes. The annotated genes were classified into 44 distinct GO terms, which are distributed across the three major functional categories: biological processes, cellular components, and molecular functions, with each GO term assigned to only one of these categories (Fig. S3). The percentage of functionally annotated genes across all Xcp isolates is shown in Fig. S4. The distribution of genes across major KEGG pathways is illustrated in Fig. S5, where they are classified as core, accessory, and unique. These genes are associated with KEGG functional modules across six groups: cellular processes, environmental information processing, genetic information processing, human diseases, metabolism, and organismal systems. Core genes are primarily mapped to metabolic pathways, followed by information processing, with minimal representation in organismal systems. Accessory genes are more prevalent in genetic information processing and metabolism compared to core and unique genes but are scarcely found in cellular processes and organismal systems. Unique genes are mainly linked to metabolism and environmental information processing, with no involvement in organismal systems. The KEGG distribution further highlights that core genes are enriched in carbohydrate and amino acid metabolism pathways but are absent from cellular communities. Unique genes are significantly associated with membrane transport, lipid metabolism, and xenobiotics biodegradation, whereas accessory genes are distinct in transcription pathways but lack connections to other pathways. Both core and unique genes contribute to biosynthesis, immune response, replication, and repair pathways (Fig. S6).

The distribution of genes across major COG pathways further categories core, accessory, and unique gene families using the COG database through BPGA (Fig. S7). Similar to the KEGG analysis, these genes were classified

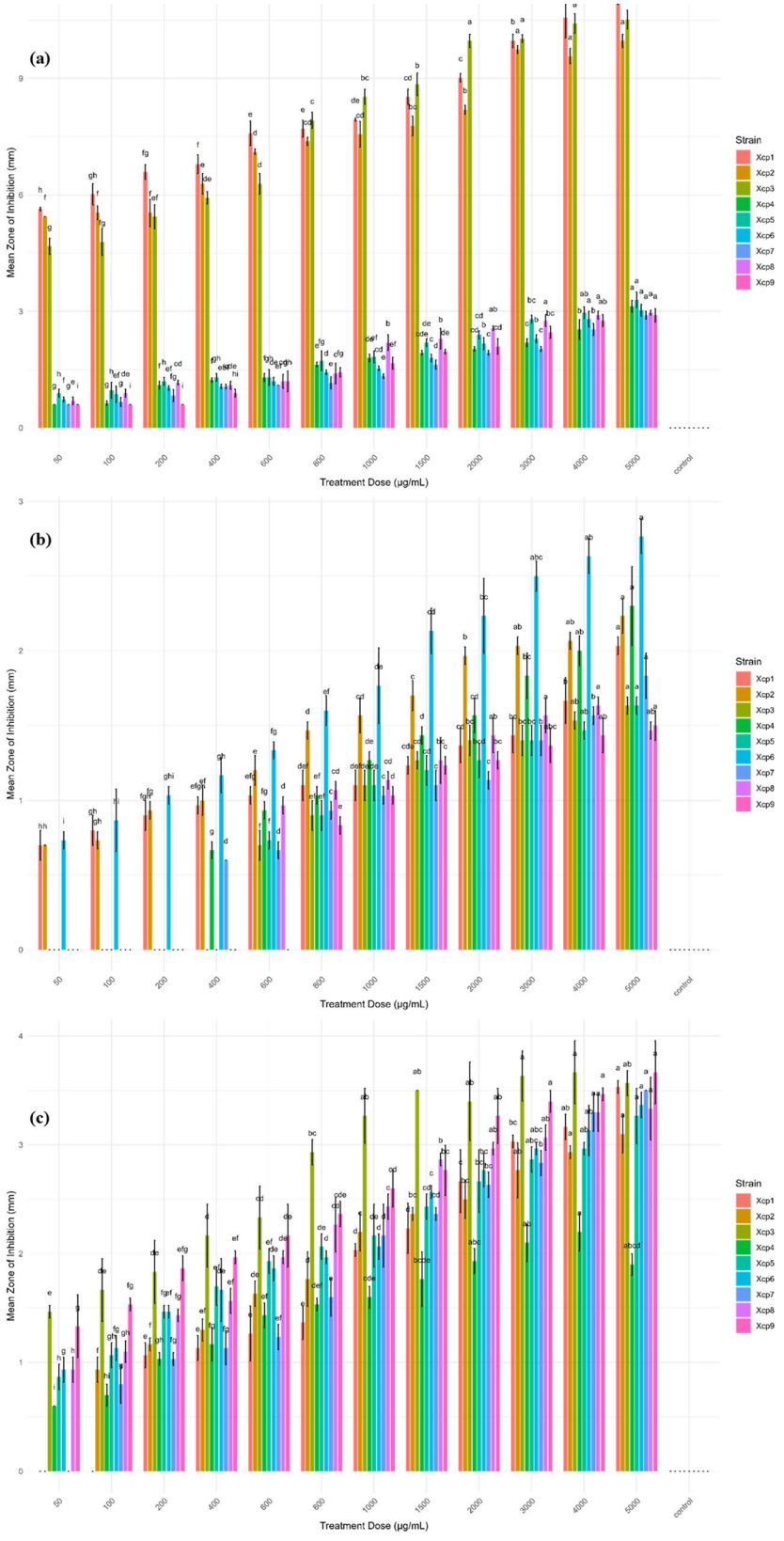

Fig. 2 Bar plot showing the mean zone of inhibition (in mm) for different antibiotic doses (**a**) streptomycin sulfate, (**b**) streptocycline, and (**c**) tetracycline against nine Xcp strains. Each bar represents the mean ± standard deviation ($n = 3$) for a given strain–dose combination, with strains Xcp1 to Xcp9 depicted in different colours. Treatments were analyzed using two-way ANOVA followed by Tukey's HSD test ($\alpha = 0.05$), where different lowercase letters above bars indicate statistically significant differences ($p < 0.05$) among treatment doses within each strain.Identical letters denote no significant difference

into functional groups related to information storage and processing, cellular processes and signalling, and metabolism, with some poorly characterized genes lacking functional assignments. Core genes were predominantly associated with metabolism, followed by cellular processes, signalling, and information storage and processing, with the lowest representation in metabolism-specific functions. Accessory and unique genes were mostly linked to information storage and processing, with accessory genes also significantly contributing to cellular processes, while unique genes were more evenly distributed across cellular processes, signaling, and metabolism. Poorly characterized genes were most common among core genes, followed by unique genes, and least frequent among accessory genes. A detailed analysis revealed that core genomes were enriched in metabolism-related functions, including general functions (Class R), lipid transport and metabolism (Class I), and secondary metabolite biosynthesis and transport (Class Q), with minimal representation in cell cycle control, defense mechanisms, and nucleotide transport (Classes D, V, and F). Accessory genes were predominantly linked to translation, ribosomal structure, and biogenesis (Class J), followed by cell wall/membrane/envelope biogenesis (Class M), with the least representation in nucleotide transport and metabolism (Class F). Notably, accessory genes were absent in functions related to cell cycle control and defense mechanisms (Classes D and V). Unique genes were highly represented in intracellular trafficking, secretion, and chaperone functions (Class U) and replication, recombination, and repair (Class L), with minimal presence in cell cycle control and coenzyme transport (Classes D and H). They showed no representation in nucleotide transport, metabolism, or defense mechanisms (Classes F and V) (Fig. S8).

The genomic islands were predicted using IslandViewer and IslandPath_DIMOB, along with their respective locations in genome sequences. The results were visualized using CGView, which generated a circular genome plot displaying contigs, GC content, and functional layers with distinct colour coding. The visualization provided insights into genome organization, pathogenicity hotspots, and resistance mechanisms as illustrated in Fig. 3a, S9.

Prediction of T3 effectors

Effectidor II analysis in pangenome mode identified 39 high-confidence effector candidates (score ≥ 0.7) in Xcp. These include conserved Xop-type effectors such as XopL, XopR, XopAE, XopN, XopK, XopQ, XopP, XopI, XopAP, and XopA, based on homology to widely studied effectors [55–57]. Notably, AvrBs2, a well-characterized avirulence/virulence effector, was also among the predictions [58]. In addition, we predicted leucine-rich repeat (LRR)-type III effectors (in XopL), XopD (which acts as a transcriptional regulator), serine/threonine kinases, transducer-like proteins, and HopG1-like effectors. A subset of hypothetical proteins lacking known domains was likewise identified, suggesting novel effector potential. The representation of both conserved and diverse predicted effectors underscores the likely importance of these proteins in the pathogenicity and virulence of *X. citri* pv. *punicae*.

T3SS components prediction

Effectidor II identified a set of genes involved in the structure of the T3SS apparatus. The first group included 17 proteins annotated as core components of the Hrp2 T3SS secretion apparatus, such as *SctE*, *SctN*, *SctF*, *SctV*, *SctU*, and *SctC*, which are critical for effector translocation. The second group comprised 24 flagellar proteins, including *fliI*, *fliM*, *flhA*, *flgH*, and *fliF*, many of which are structurally related to T3SS components due to their shared evolutionary origin. Additionally, one protein was classified as a Chlamydiales SctC-like homolog, suggesting possible horizontal gene transfer or functional mimicry. Unlike EffectiveT3, Effectidor II did not detect large numbers of hypothetical proteins, highlighting its specificity in prioritizing biologically relevant T3SS elements. While no novel effectors with canonical effector domains were detected in this dataset, the presence of complete T3SS structural genes indicates the functional integrity of the secretion system in these isolates.

Phylogenetic and evolutionary analysis of Xcp isolates

Pairwise ANI analysis confirmed that all 15 Xcp strains and reference strains share very high genomic similarity, with ANI values ranging from 98.5 to 99.9% (Fig. 4a). The heatmap is dominated by intense red shading, indicating that most strain–strain comparisons exceed 99% identity. Hierarchical clustering of ANI values resolved two major clades: one cluster groups the type strains (Xcp LMG859, Xcp LMG7439, Xcp LMG7504) together with a subset of field isolates, and the second contains the remaining isolates, including Xcp-Bagalkot and Xcp-NCPPB3563, which form a tight sub-clade. Within the latter, minor sub-structuring is apparent (e.g., Xcp 1 through Xcp 5 versus Xcp 6 through Xcp 9), suggesting subtle genetic differentiation that may reflect geographic variation.

Phylogenetic trees based on core and pan-genome analyses were constructed to illustrate the evolutionary relationships among Xcp strains using conserved genomic regions (Fig. S10). Pangenome-based phylogenetic reconstruction of our 19 Xcp genomes revealed a topology broadly concordant with the ANI and core-genome analyses, but with notable distinctions in accessory-gene clustering. In the core-genome Maximum Likelihood tree (Fig. 4b), the type strains (Xcp LMG859, Xcp

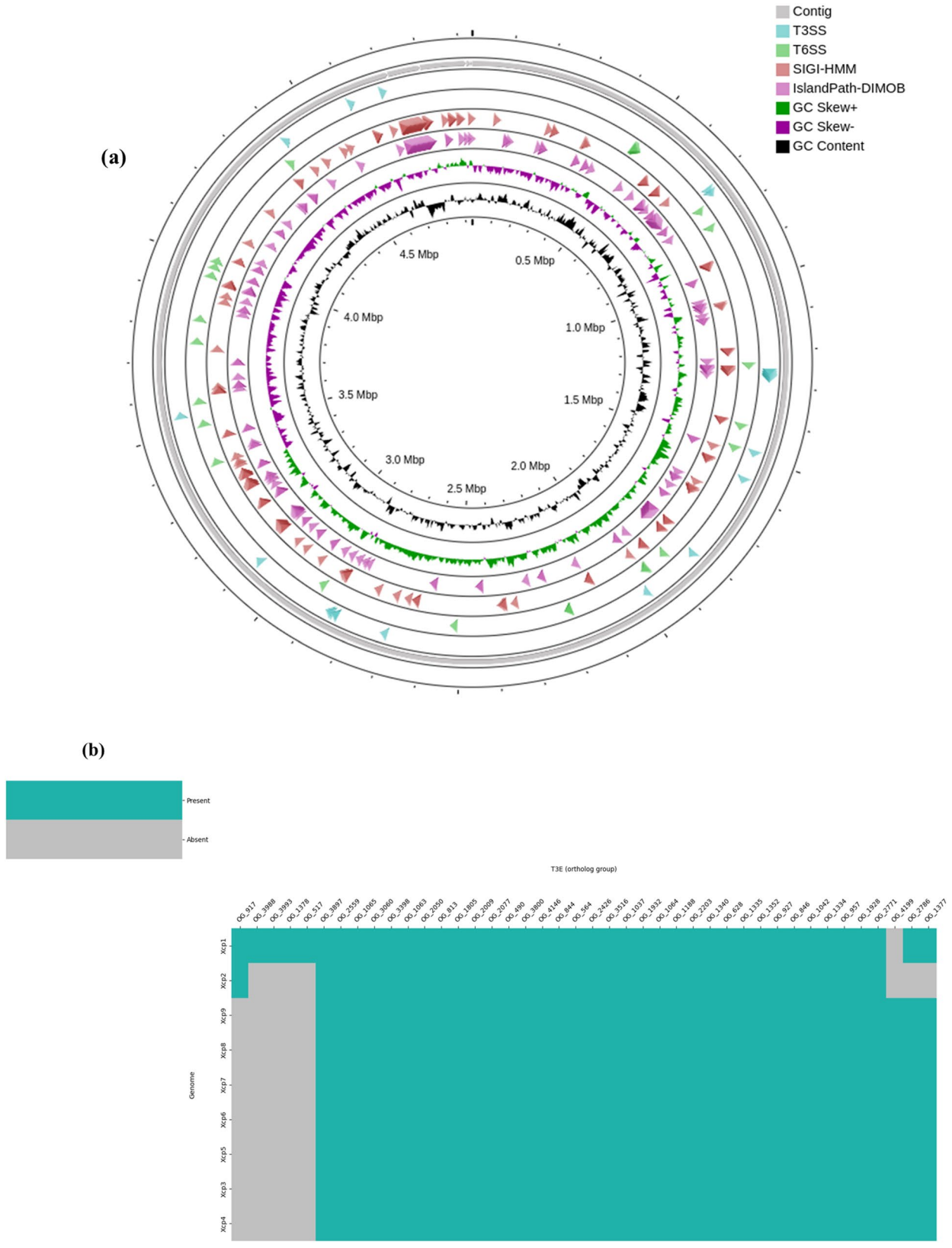

Fig. 3 **(a)** Circular genome map of Xcp1 visualized using CGView. From the outside ring to the center, Ring 2, shaded in gray, represents the contigs. Genomic islands predicted using Island Viewer are displayed with SIGI_HMM results shown in Ring 3 and Island Path_DIMOB predictions in Ring 6. Rings 4 and 5 indicate the Type III and Type VI Secretion Systems (T3SS and T6SS), as predicted by VR profile. GC skew and GC content are represented in Rings 7 and 8, respectively; (**b**) Presence–absence heatmap of selected Type III effector (T3E) genes across nine Xcp isolates

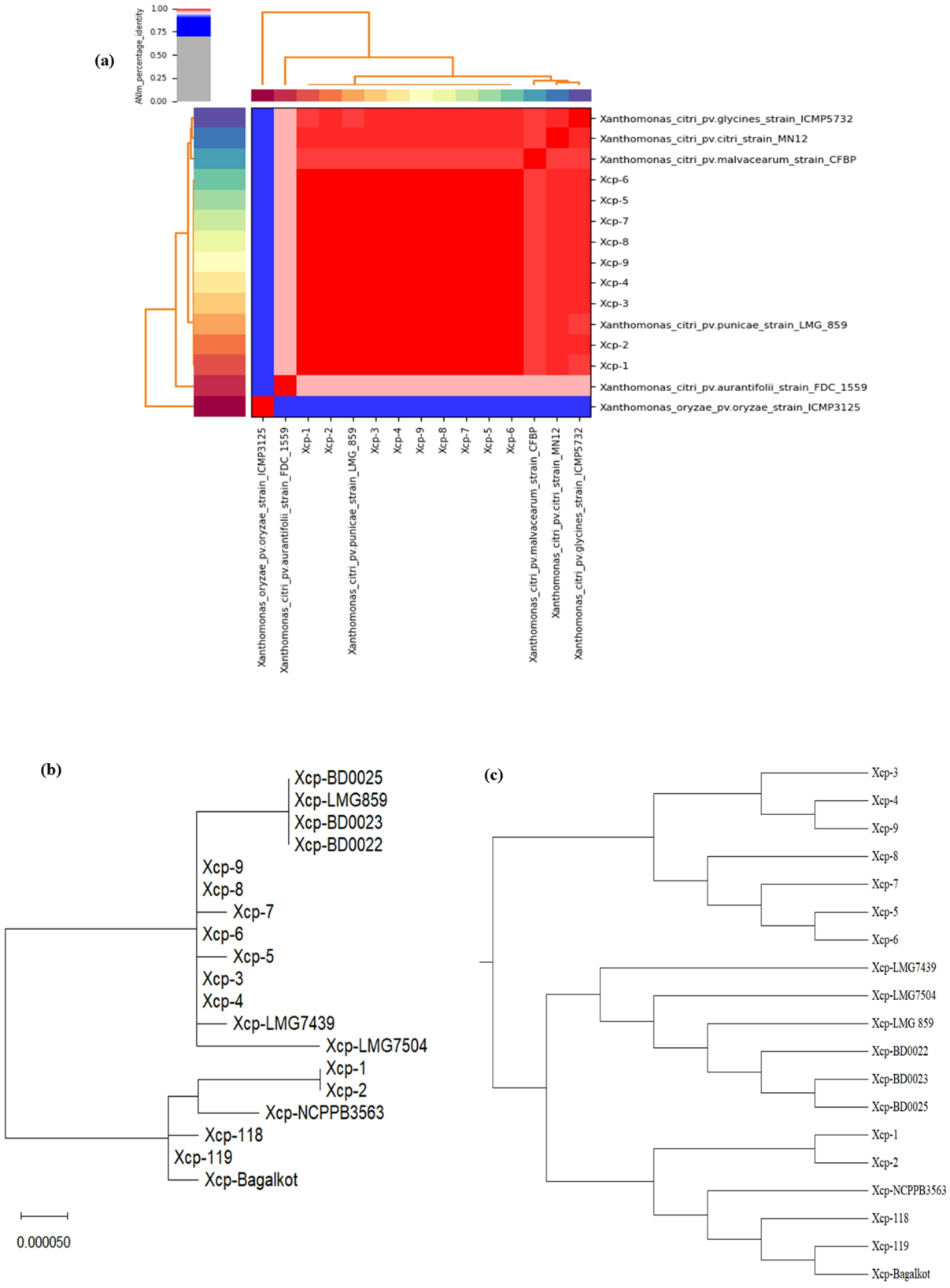

Fig. 4 **(a)** Average Nucleotide Identity (ANI) heatmap of Xcp isolates and reference strains. The heatmap illustrates pairwise ANI values among 15 Xcp isolates and reference strains. ANI values are represented using a colour gradient scale, with higher values (closer to 100%) shown in red, indicating higher genomic similarity. Hierarchical clustering was applied to both rows and columns to visualize genetic relationships, highlighting distinct clades and grouping patterns. Phylogenetic analysis of the (**b**) core genome and (**c**) accessory genes of the nine Xcp strains along with 10 reference strains

LMG7439, and Xcp LMG7504) formed a well-supported clade together with four studied strains (Xcp-BD0022, BD0023, BD0025, and Xcp-9), while a second major clade comprised Xcp 1, Xcp 2, and Xcp NCPPB3563, which in turn clustered closely with the geographically divergent strains Xcp 118, Xcp 119, and Xcp Bagalkot. Finally, a third sub-cluster grouped strains Xcp 3 through Xcp 8, reflecting subtle core-genome divergence among these closely related strains. In contrast, the accessory-gene NJ tree (Fig. 4c) based on the binary pan-matrix revealed finer sub-structuring. The BD00xx isolates remained tightly grouped but were now split into two sub-clades (BD0022/BD0023 versus BD0025), and the Xcp 3, Xcp 9 cluster subdivided into two distinct branches (Xcp 3/4/9 versus Xcp 5/6/7/8). Meanwhile, the Xcp 1/2/NCPPB3563 group and the Xcp 118/119/Bagalkot cluster each maintained their cohesion.

Detection of antibiotic-resistant genes (ARGs) across Xcp genomes

The ARG profiling of nine Xcp strains revealed the consistent presence of three chromosomal strict ARG hits across all strains, alongside a wide range of loose hits (3180–3287), suggesting the existence of diverse, putative resistance elements. Plasmid-associated resistance genes were detected in a subset of strains, with loose hits varying from 10 to 98, although no strict hits were observed on plasmids. All Xcp strains had three chromosomal genes that met the criteria for strict ARGs. The *vanY* gene from the *vanM* cluster, associated with glycopeptide resistance (vancomycin and teicoplanin), and two distinct instances of the *adeF* gene, which encodes a component of the AdeFGH efflux system conferring resistance to tetracyclines. These results indicate a stable chromosomal resistome within the Xcp population and highlight the presence of relevant resistance genes even in phytopathogenic bacteria.

Whole genomes comparison

The genome sequences of nine Xcp strains were compared to the reference whole genome of Xcp1 (5,03,4806 bp) using BRIG, as depicted in Fig. 5. The innermost circle represents the reference genome, while the outer circles of various colours correspond to the Xcp isolates. The colour shades indicate the level of similarity, with uniform shades representing complete (100%) similarity. Certain regions of the Xcp sequences showed approximately 70% similarity. Notably, regions between 4500 and 5000 kbp displayed gaps or reduced similarity (50%) across all eight Xcp isolates. Additionally, assembly breakpoints were observed near 4500 kbp in isolates Xcp2, Xcp3, Xcp4, Xcp5, and Xcp9, similar to the reference genome. However, unlike the reference genome, Xcp2 did not exhibit breakpoints near 3000 kbp.

Using the Mauve tool, the genome of Xcp1 was compared with those of Xcp2, Xcp3, Xcp4, Xcp5, Xcp6, Xcp7, Xcp8, and Xcp9. In the pairwise comparison between Xcp1 and Xcp2, the Xcp1 alignment was displayed as a single horizontal genome sequence, with a scale ranging from 0.5 Mb to 4.5 Mb. Coloured blocks above the center line represented aligned regions in the forward orientation, with similar alignment observed in Xcp2, where conserved regions were also shown as coloured blocks. Lines connecting the coloured blocks in Xcp1 and Xcp2 indicated homologous nucleotide regions between 2.0 and 2.5 Mb and 1.5–2.0 Mb.

A similar comparison between Xcp1 and Xcp3 revealed conserved mauve-coloured segments, with homologous regions identified between 2.0 and 2.5 Mb, 1.5–2.0 Mb, and additional similarity extending beyond 4.5 Mb. The Xcp1-Xcp3 comparison showed comparable alignment patterns, except for the blocks at 1.5 Mb. In the Xcp1-Xcp5 comparison, homologous regions were observed between 1.5 and 2.0 Mb and 2.0–2.5 Mb, a pattern also seen in comparisons between Xcp1 with Xcp6 as well as Xcp7.

For Xcp1-Xcp8, the alignment displayed conserved mauve-coloured regions, with homologous regions observed between 1.0 and 5.5 Mb and 2.0–2.5 Mb. The comparison between Xcp1 and Xcp9 showed a pattern similar to Xcp1 and Xcp3, with conserved regions between 2.0 and 2.5 Mb, 1.5–2.0 Mb, and additional similarity observed beyond 4.5 Mb. Overall, the pairwise genome comparisons indicated that Xcp1 shared homologous nucleotide regions with Xcp2, Xcp4, Xcp5, Xcp6, Xcp7, and Xcp8 between 2.0 and 2.5 Mb and 1.5–2.0 Mb. However, Xcp1-Xcp3, and Xcp1-Xcp9, exhibited additional genome similarity beyond 4.5 Mb, suggesting more extensive homologous regions. (Figure S12). These rearrangements and insertions observed particularly in Xcp3 and Xcp9 are likely to alter local gene content (for example, by gaining or losing genomic islands), which in turn could affect traits such as virulence, environmental adaptability, or host range. However, functional assays will be required to confirm these impacts.

Discussion

In modern high-input agriculture, antibacterial agents such as antibiotics and copper-based compounds are becoming less effective in the field, despite their past success in controlling bacterial plant pathogens. This reduced efficacy is likely due to the emergence of bactericide resistance in bacterial populations subjected to intense bactericidal pressure. Several phytopathogenic bacteria, including *X. oryzae* pv. *oryzae*, *X. campestris* pv. *vesicatoria*, *P. syringae*, *E. amylovora*, *X. alfalfae* subsp. *citrumelonis*, and *X. axonopodis* pv. *citri*, have been reported to acquire antibiotic resistance through

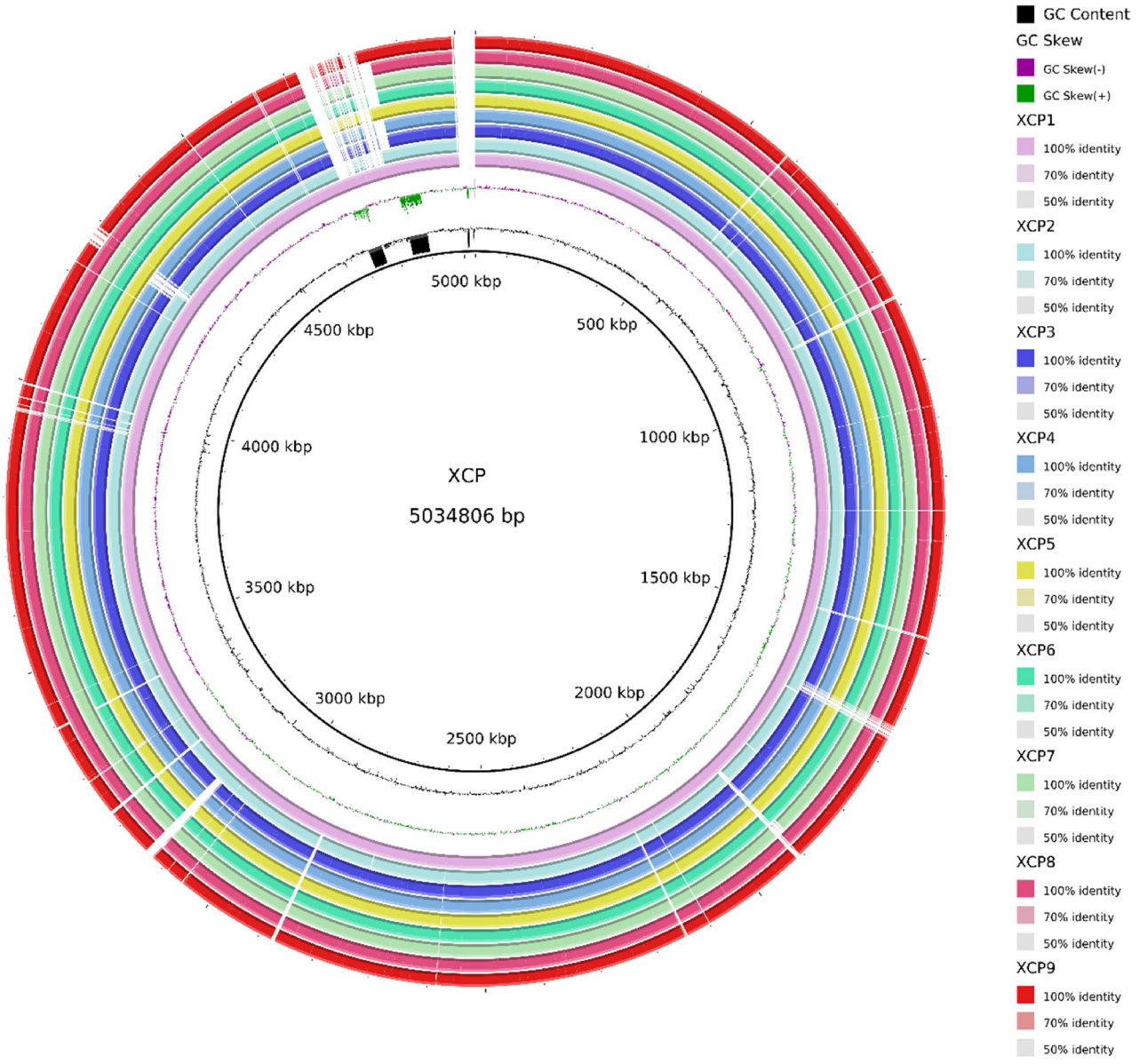

Fig. 5 Genome comparison of Xcp strains conducted using BRIG, with the hybrid de novo draft genome of Xcp1 serving as the reference against Illumina sequenced Xcp2, Xcp3, Xcp4, Xcp5, Xcp6, Xcp7, Xcp8, and Xcp9 genomes. The innermost ring represents the GC content (black), followed by the second innermost ring displaying the GC skew (purple/green). The outer rings illustrate the BLAST comparisons among the draft genomes

resistance genes. Similarly, *Xanthomonas citri* pv. *punicae* (Xcp) has shown reduced sensitivity to streptomycin and copper-based compounds [6]. The present study focused on collecting, isolating, and comprehensively characterizing Xcp to identify ARGs and other pathogenic determinants. A total of nine Xcp strains were isolated, exhibiting yellow, mucoid, and circular colony characteristics, confirming their identity as Xcp [6]. To assess their pathogenicity, different Xcp strains were inoculated onto the susceptible Bhagwa variety using the syringe method. Among them, Xcp1 was identified as the most virulent based on the lesion size. The development of typical blight symptoms further confirmed the identity of these strains as Xcp, as closely related species like *X. campestris* pv. *campestris* and *X. axonopodis* subsp. *citri* do not infect pomegranates [13].

Generally, pomegranate growers commonly use streptomycin, tetracycline, and their combination (streptocycline) in the field to control and manage the spread of Xcp. However, in recent years, farmers have reported a decline in Xcp's sensitivity to streptomycin and other antibiotics, indicating increased resistance [2]. To investigate this, the multidrug resistance profiles of Xcp isolates were assessed phenotypically using the disc diffusion assay. Two classes of antibiotics were tested: aminoglycosides (streptomycin sulfate) and tetracyclines

(tetracycline and streptocycline). Antibiotic sensitivity was assessed at a range of concentrations by measuring the zone of inhibition. While all isolates showed sensitivity to both antibiotic classes, notable differences were observed in their responses to different antibiotic concentrations. This variation may be due to their ability to withstand antibiotics effects, likely a result of selection pressure from excessive antibiotic use in the field. For individual isolates, the inhibition zone size increased with higher antibiotic concentrations, reflecting reduced bacterial growth. However, the reduction was not significant across treatments. Streptomycin sulfate and tetracycline showed greater inhibition compared to the stretocycline, though differences among isolates were observed, potentially due to the presence of streptomycin and tetracycline resistance genes. These findings suggest that Xcp isolates exhibit varied antibiotic responses and resistance to these treatments.

Advancements in sequencing technologies have simplified and significantly reduced the cost of bacterial whole genome sequencing (WGS). Unlike traditional methods, which rely on species-specific protocols and allow the analysis of only limited portions of the bacterial genome, WGS offers a comprehensive view of the entire genome. This approach provides exceptional resolution for distinguishing closely related lineages, eliminates the reliance on species-specific techniques, and uncovers additional molecular mechanisms [21]. In this study, a hybrid assembly approach combining Illumina and ONT platforms was used to assemble the genome of the Xcp1 isolate, while Illumina sequencing only was conducted for the Xcp2 to Xcp9 strains. The ANI analysis of Xcp1-9 strains revealed a high level of genomic similarity, with ANI values exceeding 99.9%, indicating close genetic relatedness among the isolates. These results corroborated the taxonomic coherence of Xcp as a single pathovar while revealing intra-species diversity that could underpin differences in virulence or adaptability. Further, the core and pan-genome phylogenetic tree highlighted the evolutionary relationships among Xcp strains. The patterns of core and accessory genes phylogenetic trees indicate that, although the core genome defines the broad species-level relationships, accessory-gene content captures additional diversity likely driven by horizontal gene transfer or niche adaptation among our Xcp strains.

Further, the comparative analysis revealed that Xcp possesses an open pan-genome, indicating a continuous acquisition of accessory genes, likely facilitated by horizontal gene transfer. This process contributes to its genomic diversity and enables strain-specific adaptations. These findings highlight the remarkable genomic plasticity of Xcp, characterized by a dynamic pan-genome driven by the addition of novel genes while maintaining a conserved core set of essential genes vital for its survival and pathogenicity.

The acquired resistance, as seen in in vitro tests, could be due to horizontal gene transfer. Genome analysis of the nine Xcp isolates identified various ARGs, with multiple predicted resistance genes spread among the isolates. These acquired ARGs are associated with resistance to various antibiotic classes, including fluoroquinolones, tetracyclines, peptides, carbapenems, macrolides, fosfomycins, aminocoumarins, monobactams, rifamycins, phenicols, aminoglycosides, nitroimidazoles, glycopeptides, lincosamides, and sulfonamides. The *adeF* gene, identified through CARD: RGI, is linked to resistance against fluoroquinolone and tetracycline antibiotics (including tetracycline and streptocycline). This gene is part of the Resistance-Nodulation-Cell Division (RND) antibiotic efflux pump family, which actively expels antibiotics from the bacterial cell, thereby reducing their effectiveness [59]. Similarly, the *tet* gene, a well-known marker of tetracycline resistance, was present in large numbers. This gene encodes a membrane-bound efflux pump responsible for actively transporting tetracycline antibiotics out of the cell, lowering their intracellular concentration and neutralizing their efficacy [60]. Additionally, loose hits for 43 aminoglycoside-class antibiotics genes were observed. The presence of these ARGs confirms the potential for resistance to tetracycline and aminoglycoside-class antibiotics, indicating the limited efficacy of these drug classes in treating infections caused by Xcp.

A whole-genome comparison of all strains was conducted to identify genetic variants contributing to their evolution. The BRIG analysis provided insights into the genomic architecture of the sequenced isolates, highlighting both conserved and divergent regions compared to the reference genome. Understanding such variations is crucial for unraveling the genetic diversity and potential functional implications within these Xcp isolates [52]. Genome comparison of Xcp isolates using the Mauve alignment tool revealed both conserved and variable genomic regions across the isolates. Pairwise alignments showed strong conservation between 1.5 and 2.5 Mbp, particularly among Xcp1, Xcp2, Xcp4, Xcp5, Xcp6, Xcp7, and Xcp8. In the region beyond 4.5 Mbp, Xcp3 and Xcp9 displayed additional homologous blocks not present in other isolates, indicating possible structural variations such as insertions or rearrangements. In contrast, the apparent breakpoints observed in Xcp2, Xcp4, and Xcp5 in the same region corresponded with contig boundaries and lacked syntenic rearrangement, suggesting they are likely assembly artifacts caused by repetitive sequences or low coverage. These observations are consistent with findings by Jalali et al. (2018), who reported genome rearrangements, gene duplications, and losses primarily

involving transposase genes and hypothetical proteins between two Iranian *Xanthomonas citri* strains, while core pathogenicity and virulence genes remained largely conserved [61].

Conclusion

This study underscores the growing challenge of antibiotic resistance in Xcp, which has significant implications in pomegranate farming. The phenotypic and genomic analyses revealed significant variability in antibiotic sensitivity among Xcp isolates, likely driven by horizontal gene transfer and selection pressure from excessive antibiotic application. WGS and comparative genomics provided deep insights into the genetic diversity, evolutionary mechanisms, and accessory gene contributions to resistance and pathogenicity. The presence of diverse ARGs and dynamic pan-genome adaptations highlight the pathogen's remarkable genomic plasticity, emphasizing the need for integrated management strategies. These findings lay the foundation for future research on developing targeted strategies to manage antibiotic-resistant strains of Xcp.

Supplementary Information

The online version contains supplementary material available at https://doi.org/10.1186/s12866-025-04625-w.

Supplementary Material 1.

Supplementary Material 2.

Supplementary Material 3.

Supplementary Material 4.

Supplementary Material 5.

Acknowledgements
The authors gratefully acknowledge the University of Agricultural Sciences, GKVK, Bengaluru, for all the support rendered for the smooth conduct of research.

Authors' contributions
Conceptualization: M.K.P.; Writing – original draft: RV., A.K.; Investigation: C.M., P.D., H.B.M.; Formal analysis: R.K., G.V., H.J., S.N.B., S.S.P.; Software: A.N.S., K.V., S.R., A.K., Writing – review and editing: R.Y.S., S.K.

Funding
This research did not receive any specific grant from funding agencies in the public, commercial, or not-for-profit sectors.

Data availability
The whole genome sequencing data for Xcp isolates (Xcp1–Xcp9) have been deposited in the NCBI GenBank database under the accession numbers JAODJP000000000, JAODJO000000000, JAODJN000000000, JAODJM000000000, JAODJL000000000, JAODJK000000000, JAODJJ000000000, JAODJI000000000, and JAODJH000000000. All isolates are linked to BioProject ID PRJNA865108 and have corresponding BioSample accession numbers SAMN30096794–SAMN30096802. These data are publicly accessible via the NCBI database. Additionally, the raw sequencing reads have been submitted to the NCBI SRA database with the following accession numbers: SRR35018596 (Xcp1 – Illumina), SRR35290729 (Xcp1 – Nanopore), SRR35018595 (Xcp2), SRR35018594 (Xcp3), SRR35018593 (Xcp4), SRR35018592 (Xcp5), SRR35018591 (Xcp6), SRR35018590 (Xcp7), SRR35018589 (Xcp8), and SRR35018588 (Xcp9). Additionally, the Prokka annotation files used in our analyses, are provided as supplementary material to ensure reproducibility alongside the PGAP annotations available at NCBI.

Declarations

Ethics approval and consent to participate
Not applicable.

Consent for publication
Not applicable.

Competing interests
The authors declare no competing interests.

Author details
[1]PathoGenomics Laboratory, Department of Plant Pathology, University of Agricultural Sciences, GKVK, Bengaluru, Karnataka 560 065, India
[2]ICAR- National Bureau of Agricultural Insect Resources, Bengaluru, Karnataka 560 024, India
[3]ICAR-Directorate of Mushroom Research, Solan, Himachal Pradesh 173 213, India
[4]BaseSolve Informatics Pvt. Ltd., Ahmedabad, Gujarat 380 059, India
[5]Agroforestry Development Centre, Agriculture and Agri-Food Canada, Indian Head, SK K1A 0C5, Canada
[6]Aquatic and Crop Resource Development, National Research Council Canada, Saskatoon, SK S7N 0W9, Canada

Received: 27 March 2025 / Accepted: 10 December 2025
Published online: 16 January 2026

References

1. Sivaraman S, Krishnamoorthy D, Arvind K, Grace T, Sharma J, Antony G. TAL effectors and the predicted host targets of pomegranate bacterial blight pathogen *Xanthomonas citri* pv. *punicae*. Curr Genet. 2022;68(3–4):361–73. https://doi.org/10.1007/s00294-022-01191-9.
2. Sharma J, Manjunatha N, Pokhare SS, Patil PG, Agarrwal R, Chakranarayan MG, et al. Genetic diversity and streptomycin sensitivity in *Xanthomonas axonopodis* pv. *punicae* causing oily spot disease in pomegranates. Horticulturae. 2022;8(5):441. https://doi.org/10.3390/horticulturae8050441.
3. Singh NV, Parashuram S, Sharma J, Potlannagari RS, Karuppannan DB, Pal RK, et al. Comparative transcriptome profiling of pomegranate genotypes having resistance and susceptible reaction to *Xanthomonas axonopodis* pv. *punicae*. Saudi J Biol Sci. 2020;27(12):3514–28. https://doi.org/10.1016/j.sjbs.2020.08.005.
4. Kumar K, Jyotsana S, Vilas S, Jadhav T. Status of bacterial blight of pomegranate in India. Fruit Veg Cereal Sci Biotechnol. 2010;4:102–5.
5. Radhika DH, Gunnaiah R, Lamani A, Peerjade D, Jagadeesha RC. Long-read genome sequence resources of *Xanthomonas citri* pv. *punicae* strain Bagalkot causing pomegranate bacterial blight. Mol Plant-Microbe Interact. 2021;34(7):874–7. https://doi.org/10.1094/MPMI-04-21-0081-A.
6. Krishna P, Kumar MP, Channappa M, Devanna P, Singh K, Eeregowda PM, et al. Antibiotic resilience in *Xanthomonas axonopodis* pv. *punicae* causing bacterial blight of pomegranate. Curr Sci. 2020;119(9):1564–9.
7. Araujo ER, Pereira RC, Ferreira MASV, Quezado-Duval AM, Café-Filho AC. Sensitivity of Xanthomonads causing tomato bacterial spot to copper and streptomycin and in vivo infra-specific competitive ability in *Xanthomonas perforans* resistant and sensitive to copper. J Plant Pathol. 2012;94(1):79–87.
8. Behlau F, Jones JB, Myers ME, Graham JH. Monitoring for resistant populations of Xanthomonas citri subsp. citri and epiphytic bacteria on citrus trees treated with copper or streptomycin using a new semi-selective medium. Eur J Plant Pathol. 2012;132:259–70. https://doi.org/10.1007/s10658-011-9865-0.
9. Xu Y, Zhu XF, Zhou MG, Kuang J, Zhang Y, Shang Y, et al. Status of streptomycin resistance development in Xanthomonas oryzae pv. oryzae and Xanthomonas oryzae pv. oryzicola in China and their resistance characters. J Phytopathol. 2010;158(9):601–8. https://doi.org/10.1111/j.1439-0434.2010.01673.x.

10. Potnis N, Timilsina S, Strayer A, Shantharaj D, Barak JD, Paret ML, et al. Bacterial spot of tomato and pepper: diverse *Xanthomonas* species with a wide variety of virulence factors posing a worldwide challenge. Mol Plant Pathol. 2015;16(9):907–20. https://doi.org/10.1111/mpp.12244.
11. Roach R, Mann R, Gambley CG, Chapman T, Shivas RG, Rodoni B. Genomic sequence analysis reveals diversity of Australian *Xanthomonas* species associated with bacterial leaf spot of tomato, capsicum, and Chilli. BMC Genomics. 2019;20:1–22. https://doi.org/10.1186/s12864-019-5600-x.
12. Kumar R, Mondal KK. XopN-T3SS effector modulates in planta growth of *Xanthomonas axonopodis* pv. *punicae* and cell-wall-associated immune response to induce bacterial blight in pomegranate. Physiol Mol Plant Pathol. 2013;84:36–43. https://doi.org/10.1016/j.pmpp.2013.06.002.
13. Doddaraju P, Kumar P, Gunnaiah R, Gowda AA, Lokesh V, Pujer P, et al. Reliable and early diagnosis of bacterial blight in pomegranate caused by *Xanthomonas axonopodis* pv. *punicae* using sensitive PCR techniques. Sci Rep. 2019;9:p10097. https://doi.org/10.1038/s41598-019-46588-9.
14. R Core Team. R: A language and environment for statistical computing. R Foundation for Statistical Computing, Vienna, Austria. 2016. https://www.R-project.org/. Accessed 15 Dec 2024.
15. Wickham H, François R, Henry L, Müller K, Vaughan D. dplyr: A Grammar of Data Manipulation. R package version 1.1.4. 2025. https://dplyr.tidyverse.org. Accessed 15 Dec 2024.
16. Wickham H, Vaughan D, Girlich M. tidyr: Tidy Messy Data. R package version 1.3.1. 2025. https://tidyr.tidyverse.org. Accessed 15 Dec 2024.
17. Wickham H. ggplot2: Elegant Graphics for Data Analysis. Springer-Verlag New York. 2016. ISBN 978-3-319-24277-4. https://doi.org/10.1007/978-0-387-98141-3.
18. Thompson JD, Higgins DG, Gibson TJ. CLUSTAL W: improving the sensitivity of progressive multiple sequence alignment through sequence weighting, position-specific gap penalties and weight matrix choice. Nucleic Acids Res. 1994;22(22):4673–80. https://doi.org/10.1093/nar/22.22.4673.
19. Hall TA. BioEdit: a user-friendly biological sequence alignment editor and analysis program for Windows 95/98/NT. In Nucleic acids symposium series. 1999;41:95–98.
20. Tamura K, Stecher G, Kumar S. MEGA11: molecular evolutionary genetics analysis version 11. Mol Biol Evol. 2021;38(7):3022–7. https://doi.org/10.1093/molbev/msab120.
21. Kukreti A, Kotasthane AS, Tandon AL, Nekkanti A, Prasannakumar MK, Devanna P, et al. Hybrid de Novo whole-genome assembly of lipopeptide-producing novel *Bacillus Thuringiensis* strain NBAIR BtAr exhibiting antagonistic activity against *Sclerotium rolfsii*. Microb Pathog. 2024;195:106867. https://doi.org/10.1016/j.micpath.2024.106867.
22. Andrews S. FastQC: a quality control tool for high throughput sequence data. 2010. https://www.bioinformatics.babraham.ac.uk/projects/fastqc/. Accessed 15 Dec 2024.
23. Chen S, Zhou Y, Chen Y, Gu J. Fastp: an ultra-fast all-in-one FASTQ preprocessor. Bioinformatics. 2018;34(17):i884–90. https://doi.org/10.1093/bioinformatics/bty560.
24. Bolger AM, Lohse M, Usadel B. Trimmomatic: a flexible trimmer for illumina sequence data. Bioinformatics. 2014;30:2114–20. https://doi.org/10.1093/bioinformatics/btu170.
25. De Coster W, D'Hert S, Schultz DT, Cruts M, Van Broeckhoven C. NanoPack: visualizing and processing long-read sequencing data. Bioinformatics. 2018;34(15):2666–9. https://doi.org/10.1093/bioinformatics/bty149.
26. Wick RR, Judd LM, Gorrie CL, Holt KE. Unicycler: resolving bacterial genome assemblies from short and long sequencing reads. PLoS Comput Biol. 2017;13(6):e1005595. https://doi.org/10.1371/journal.pcbi.1005595.
27. Alonge M, Soyk S, Ramakrishnan S, et al. RaGOO: fast and accurate reference-guided scaffolding of draft genomes. Genome Biol. 2019;20:224. https://doi.org/10.1186/s13059-019-1829-6.
28. Souvorov A, Agarwala R, Lipman DJ. SKESA: strategic k-mer extension for scrupulous assemblies. Genome Biol. 2018;19(1):1–13. https://doi.org/10.1186/s13059-018-1540-z.
29. Kang DD, Li F, Kirton E, Thomas A, Egan R, An H, et al. MetaBAT 2: an adaptive Binning algorithm for robust and efficient genome reconstruction from metagenome assemblies. PeerJ. 2019;7:e7359. https://doi.org/10.7717/peerj.7359.
30. Parks DH, Imelfort M, Skennerton CT, Hugenholtz P, Tyson GW. CheckM: assessing the quality of microbial genomes recovered from isolates, single cells, and metagenomes. Genome Res. 2015;25(7):1043–55. https://doi.org/10.1101/gr.186072.114.
31. Gurevich A, Saveliev V, Vyahhi N, Tesler G. QUAST: quality assessment tool for genome assemblies. Bioinformatics. 2013;29(8):1072–5. https://doi.org/10.1093/bioinformatics/btt086.
32. Seemann T. Prokka: rapid prokaryotic genome annotation. Bioinformatics. 2014;30(14):2068–9. https://doi.org/10.1093/bioinformatics/btu153.
33. Tanizawa Y, Fujisawa T, Nakamura Y. DFAST: a flexible prokaryotic genome annotation pipeline for faster genome publication. Bioinformatics. 2018;34(6):1037–9. https://doi.org/10.1093/bioinformatics/btx713.
34. Jehl MA, Arnold R, Rattei T. Effective—a database of predicted secreted bacterial proteins. Nucleic Acids Res. 2010;39:D591–5. https://doi.org/10.1093/nar/gkq1158.
35. Schwengers O, Barth P, Falgenhauer L, Hain T, Chakraborty T, Goesmann A. Platon: identification and characterization of bacterial plasmid contigs in short-read draft assemblies exploiting protein sequence-based replicon distribution scores. Microb Genom. 2020;6(10). https://doi.org/10.1099/mgen.0.000398.
36. Toronen P, Medlar A, Holm L. PANNZER2: a rapid functional annotation web server. Nucleic Acids Res. 2018;46(W1):W84–8. https://doi.org/10.1093/nar/gky350.
37. Ye J, Zhang Y, Cui H, Liu J, Wu Y, Cheng Y, et al. WEGO 2.0: a web tool for analyzing and plotting GO annotations, 2018 update. Nucleic Acids Res. 2018;46(W1):W71–5. https://doi.org/10.1093/nar/gky400.
38. Venu HS, Shylesha AN, Ruqiya S, Rangeshwaran R, Manjunatha C, Kandan A, et al. Bioefficacy and molecular characterization of *Bacillus Thuringiensis* strain NBAIR BtGa against greater wax moth, *Galleria Mellonella* L. Braz J Microbiol. 2024;1–9. https://doi.org/10.1007/s42770-023-00716-5.
39. Li J, Tai C, Deng Z, Zhong W, He Y, Ou HY. VRprofile: gene-cluster-detection-based profiling of virulence and antibiotic resistance traits encoded within genome sequences of pathogenic bacteria. Brief Bioinform. 2018;19(4):566–74. https://doi.org/10.1093/bib/bbx019.
40. Lee I, Kim YO, Park SC, Chun J. OrthoANI: an improved algorithm and software for calculating average nucleotide identity. Int J Syst Evol Microbiol. 2016;66(2):1100–3. https://doi.org/10.1099/ijsem.0.000760.
41. Varani AM, Siguier P, Gourbeyre E, Charneau V, Chandler M. ISsaga: an ensemble of web-based methods for high throughput identification and semi-automatic annotation of insertion sequences in prokaryotic genomes. Genome Biol. 2011;12(3):R30. https://doi.org/10.1186/gb-2011-12-3-r30.
42. Hawkey J, Hamidian M, Wick RR, Edwards DJ, Billman-Jacobe H, Hall RM, et al. ISMapper: identifying transposase insertion sites in bacterial genomes from short-read sequence data. BMC Genomics. 2015;16:1–11. https://doi.org/10.1186/s12864-015-1459-3.
43. Seemann T. Rapid haploid variant calling and core genome alignment. Snippy. 2019. Available from. https://github.com/tseemann/snippy
44. Bertelli C, Laird MR, Williams KP, Simon Fraser University Research Computing Group, Lau BY, Hoad G, Brinkman FS. IslandViewer 4: expanded prediction of genomic Islands for larger-scale datasets. Nucleic Acids Res. 2017;45(W1):W30–5. https://doi.org/10.1093/nar/gkx334.
45. Chaudhari NM, Gupta VK, Dutta C. BPGA-an ultra-fast pan-genome analysis pipeline. Sci Rep. 2016;6:24373. https://doi.org/10.1038/srep24373.
46. Jones DT, Taylor WR, Thornton JM. The rapid generation of mutation data matrices from protein sequences. Bioinformatics. 2022;8:275–82. https://doi.org/10.1093/bioinformatics/8.3.275.
47. Dereeper A, Summo M, Meyer DF. PanExplorer: a web-based tool for exploratory analysis and visualization of bacterial pan-genomes. Bioinformatics. 2022;38:4412–4. https://doi.org/10.1093/bioinformatics/btac504.
48. Wagner N, et al. Effectidor II: a pan-genomic AI-based algorithm for the prediction of type III secretion system effectors. Bioinformatics. 2025;41(5). https://doi.org/10.1093/bioinformatics/btaf272.
49. Krawczyk PS, Lipinski L, Dziembowski A. PlasFlow: predicting plasmid sequences in metagenomic data using genome signatures. Nucleic Acids Res. 2018;46(6):e35–35. https://doi.org/10.1093/nar/gkx1321.
50. Alcock BP, et al. CARD 2020: antibiotic resistome surveillance with the comprehensive antibiotic resistance database. Nucleic Acids Res. 2020;48(D1):D517–25. https://doi.org/10.1093/nar/gkz935.
51. Grant JR, Enns E, Marinier E, Mandal A, Herman EK, Chen CY, et al. Proksee: in-depth characterization and visualization of bacterial genomes. Nucleic Acids Res. 2023;51(W1):W484–92. https://doi.org/10.1093/nar/gkad326.
52. Alikhan NF, Petty NK, Ben Zakour NL, Beatson SA. BLAST ring image generator (BRIG): simple prokaryote genome comparisons. BMC Genomics. 2011;12:40. https://doi.org/10.1186/1471-2164-12-40.

53. Altschul SF, Gish W, Miller W, Myers EW, Lipman DJ. Basic local alignment search tool. J Mol Biol. 1990;215:403–10. https://doi.org/10.1016/S0022-2836(05)80360-2.
54. Darling AC, Mau B, Blattner FR, Perna NT. Mauve: multiple alignment of conserved genomic sequence with rearrangements. Genome Res. 2004;14(7):1394–403. https://doi.org/10.1101/gr.2289704.
55. Soni M, Mondal KK. *Xanthomonas axonopodis* pv. *punicae* uses XopL effector to suppress pomegranate immunity. J Integr Plant Biol. 2018;60(4):341–57. https://doi.org/10.1111/jipb.12615.
56. Ma W, Xu X, Cai L, Cao Y, Haq F, Alfano JR, et al. A type III effector XopL from *Xanthomonas oryzae* causes cell death by mediating ferredoxin degradation in *Nicotiana benthamiana*. Phytopathol Res. 2020;2:16. https://doi.org/10.1186/s42483-020-00055-w.
57. Wang S, Sun J, Fan F, Tan Z, Zou Y, Lu D. A Xanthomonas oryzae pv. oryzae effector, XopR, associates with receptor-like cytoplasmic kinases and suppresses PAMP-triggered stomatal closure. Sci China Life Sci. 2016;59(9):897–905. https://doi.org/10.1007/s11427-016-5106-6.
58. Li S, Wang Y, Wang S, Fang A, Wang J, Liu L, et al. The type III effector AvrBs2 in Xanthomonas oryzae pv. oryzicola suppresses rice immunity and promotes disease development. Mol Plant Microbe Interact. 2015;28(8):869–80.
59. Coyne S, Rosenfeld N, Lambert T, Courvalin P, Périchon B. Overexpression of resistance-nodulation-cell division pump AdeFGH confers multidrug resistance in *Acinetobacter baumannii*. Antimicrob Agents Chemother. 2010;54:4389–93. https://doi.org/10.1128/aac.00155-10.
60. Chopra I, Roberts M. Tetracycline antibiotics: mode of action, applications, molecular biology, and epidemiology of bacterial resistance. Microbiol Mol Biol Rev. 2001;65:232–60. https://doi.org/10.1128/mmbr.65.2.232-260.2001.
61. Jalali A, Alavi SM, Sangtarash MH. Genomic characterization and phylogenetic analysis of a narrow host-range Iranian strain of *Xanthomonas citri* subsp. *citri*, NIGEB-88. J Microb World. 2018;11. https://www.researchgate.net/publication/325119449_Genomic_characterization_and_phylogenetic_analysis_of_a_narrow_host_rang_Iranian_strain_of_Xanthmonas_citri_sub_citri_NIGEB-88}

Publisher's note